Label-Free Sensing of Biorecognition on Liposomes

Rasmussen, Martin Kjærulf; Pedersen, Jonas Nyvold; Marie, Rodolphe

Published in:
ACS Sensors

Link to article, DOI:
10.1021/acssensors.0c02120

Publication date:
2020

Document Version
Peer reviewed version

Label-free Sensing of Biorecognition on Liposomes

Martin K. Rasmussen, Jonas N. Pedersen,* and Rodolphe Marie*

Department of Health Technology, Technical University of Denmark, 2800 Kongens Lyngby, Denmark

E-mail: J.N.P:jnpe@dtu.dk; R.M:rcwm@dtu.dk

Abstract

Nanometer-sized liposomes decorated with macromolecules are increasingly used as drug delivery vehicles due to their long lifetimes and target-cell specificity, but surface characterization methods often change their properties which leads to incorrect results. Ligand binding is commonly applied for characterizing these surface modifications. Here we use a nanofluidic-based, label-free sensor for real-time sensing of ligands binding to liposomes. The liposomes are trapped in a nanochannel with a salt concentration gradient, and as the trapping position depends on the liposomes' zeta potential, it changes when charged ligands bind to the liposomes. Our sensing method does not require immobilization of the liposomes or labeling of the ligands with fluorophores, which may both affect the sensing. The zeta potential sensing is demonstrated by measuring hybridization of DNA targets with complementary DNA probes on liposome surfaces. DNA hybridization is monitored for both ensembles and individual liposomes, the latter allows for analysis of ensemble heterogeneity, and we demonstrate sensitivity to changes in surface charge down to 1.5%. DNA hybridization is used to demonstrate label-free sensing, but the method also has potential applications within exosome char-

acterization, where biorecognition of, e.g., surface DNA, proteins, and antibodies is a promising candidate for early stage cancer diagnostics.

Keywords: Nanofluidic sensor, Mimetic membranes, Label-free, Immobilization-free, Diffusiophoresis, Drug Delivery, Zeta potential

Soft matter colloids such as liposomes and micelles are frequently used as drug delivery vehicles and as mimetic membranes for studying the interactions of small drug molecules with cell membranes [1–3]. Designing liposomes as efficient drug delivery carriers routinely involves modifications of their surface properties for which different strategies are pursued [4,5]. For example, coating of liposomes with polymer brushes protects the liposomes from phagocytic cells thus increasing their lifetime *in vivo* [4], and functionalization with ligands such as peptides [6,7], antibodies [8,9] and DNA [5] allows for targeting receptors on specific cells. Liposomes modified with DNA are also crucial for studying reactions of subattoliter volumes of reagents by liposome fusion [10,11].

Characterizing the surface modifications of self-assembled colloids is key to their rational design and motivates the development of a number of sensing methods. Fluorescence-based assays are widely used, but they often require fluorescent labeling of the ligand which can influence its binding properties [12]. Hence label-free techniques such as Localized Surface Plasmon Resonance (L-SPR) [13] and Quartz Crystal Microbalance with Dissipation monitoring (QCM-D) [14] are attractive alternatives, but they require immobilization of the colloids on a surface or replace the colloids by supported lipid membranes. The immobilization can change the lipid membrane permeability and fluidity [15], and supported membranes have no curvature which may be an integral part of the binding process [16,17]. Moreover, all these methods are based on ensembles of colloids, and they are challenged if several sub-populations of colloids with different properties are present in the ensemble [18].

Many ligands are charged, so monitoring the change in surface charge is an attractive route for measuring functionalization [19–21]. Surface charge can be probed with, e.g., Laser

Doppler Electrophoresis (LDE) [22] and Second Harmonic Generation (SHG) [20], however both methods probe ensemble properties. Tunable Resistive Pulse Sensing (TRPS) measures size and surface charge for individual particles with diameters down to $\sim 70\,\mathrm{nm}$ diameters before and after functionalization of an ensemble, but the functionalization must be done outside of the assay, which prevents real-time monitoring of single particles [23]. Single-molecule electrometry has been demonstrated for both DNA and proteins, but it is carried out at low ionic strengths which prevents biochemical reactions to be performed at physiological salinity [24,25].

In summary, there is a need for methods which are label-free, without the need for immobilization, and which is able to analyze subpopulations of liposomes at physiological conditions.

Here we monitor binding of target molecules to functionalized liposomes in a nanofluidic sensor in real-time. The liposomes are functionalized with double-stranded DNA (dsDNA) probes with a single stranded overhang, and they are only exposed to complementary single-stranded DNA (ssDNA) targets while trapped. The trapping occurs in a nanochannel with an imposed salinity gradient [26], which causes a diffusioosmotic fluid flow and an oppositely directed diffusiophoretic particle transport [27]. So trapping happens where the flow and the particle velocities balance. The spatial distribution of the trapped liposomes depends on their surface characteristics as the diffusiophoretic particle transport is a function of the liposomes' surface charges and diameters. Hence the distribution changes as probes on the liposome surfaces are hybridized. Note that the liposomes, not the target molecules, are fluorescently labeled. This provides a clear optical signal that is independent of the number of targets bound to the probes, and binding is observed without labeling the targets. We first demonstrate how to quantify the number of probes on an ensemble of liposomes (Figure 1). Then we show how the hybridization of complementary DNA targets is monitored in real-time for an ensemble of liposomes (Figure 2). Finally, the hybridization is monitored on individual liposomes (Figure 3).

RESULTS AND DISCUSSION

Liposomes with the fluorescent dye DiO were prepared by lipid film hydration from a membrane with a lipid composition of POPC (1-palmitoyl-2- oleoyl-glycero-3-phosphocholine) and POPG (1-palmitoyl-2-oleoyl- sn-glycero-3-phosphoglycerol) in a 3:1 ratio and extruded through a membrane with 30 nm holes (details in EXPERIMENTAL SECTION). The mean diameter of the resulting liposomes is 76 nm, as measured by DLS. The DNA probes were made by hybridizing two ssDNA molecules, 12 and 27 bases long, with cholesterol (CH) tags at the 3' and 5' ends, respectively (Figure 1a). This creates a double CH anchor on one side and a 15-base single-stranded overhang on the opposite side. The cholesterol ensures strong binding of the probes to liposome bilayers [28]. Liposomes are mixed with different concentrations of DNA probes to create four samples with 27 ± 4, 44 ± 7, 260 ± 30 and 620 ± 50 DNA probes per liposome. The number of DNA probes per vesicle were measured by an independent fluorescence bleaching experiment (Figure S2).

Then the liposomes were introduced in the nanofludic sensor shown schematically in Figure 1b (details in Supporting Information). The nanofluidic sensor consists of funnel-shaped nanochannels connecting two microchannnels. Each nanochannel is 295 nm high, 5 µm wide at the narrow end, and 20 µm at the wide end. Continuous flows of buffers with different salinities in the two microchannels maintain a constant salt gradient across the nanochannels. Phosphate buffered saline (PBS) concentrations are $C_N = 10^{-3}\times$PBS and $C_W = 10\times$PBS at the narrow and wide ends of the nanochannels, respectively. The gradient causes a diffusioosmotic liquid flow with a velocity $v_{\mathrm{os}}(x)$ that varies along the nanochannel due to the changing cross-sectional area of the nanochannel (Supporting Information and Figure S1) [29].

The liposomes were added to the nanochannels by replacing the buffer in the microchannel with a low salt concentration (C_N) with a solution having the same salt concentration but also containing DNA probes. This leaves the salt gradient, and hence the trapping position, unaffected. As the liposomes pass the narrow end of the nanochannels, some liposomes

spontaneously enter the nanochannels due to diffusiophoresis [27,30]. Inside the nanochannel, the velocity of the diffusiophoretic motion of the liposomes $v_{\mathrm{ph}}(x)$ is opposite to the direction of the fluid $v_{\mathrm{os}}(x)$ (details in Supporting Information Section 1). So liposomes get trapped where the two velocities balance (Movie S1). The ionic strengths in the microchannels are chosen so that trapping occurs near physiological conditions, i.e. $\sim 1\times$PBS and a Debye length of $\sim 1\,\mathrm{nm}$. This is important for biochemical reactions, e.g., DNA hybridization.

We trap ensembles of liposomes with different numbers of DNA probes in the nanochannels (Figure 1c). A higher number of DNA probes causes a trapping position further into the nanochannel, as the negatively charged probes makes the liposomes' zeta potential more negative, which increases the diffusiophoretic velocity $v_{\mathrm{ph}}(x)$ [26]. Note that although liposomes are trapped, they still move around the average trapping position due to Brownian motion. This results in a smeared distribution of liposomes in the nanochannel. The width of the smeared distribution depends on the particles' diffusion coefficient, but also on the trapping position as the diffusiophoretic and diffusioosmotic velocities change along the funnel-shaped nanochannel.

From the microscopy images in Figure 1c, we extract the average intensity $I(x)$ across the nanochannel versus the position along the nanochannel (dots in Figure 1d). We then fit the intensity to an expression for the equilibrium distribution of liposomes in the nanochannel [26],

$$I(x) = I(x_0) e^{\int_{x_0}^{x} dx' \, [v_{\mathrm{os}}(x') + v_{\mathrm{ph}}(x')]/D_p}. \tag{1}$$

Here $I(x_0)$ is the fluorescence intensity at the trapping position x_0, and the diffusioosmotic velocity $v_{\mathrm{os}}(x)$ is known from an independent characterization of the sensor (see Supporting Information Section 1). The diffusion coefficient for a particle confined between two infinite parallel plates $D_p = D_p(d)$ depends on the diameter d of the liposomes[26,31], while the diffusiophoretic velocity $v_{\mathrm{ph}} = v_{\mathrm{ph}}(d, \zeta)$ depends on both the liposomes' diameter and the zeta potential ζ. So a fit of the measured intensity profile to eq 1, has d and ζ as the only free

parameters, except for a scaling parameter $I(x_0)$ that relates the intensity to the number of trapped liposomes. Fits are marked with full lines in Figure 1d, and fitted values for ζ are shown Figure 1e. For bare liposomes without DNA probes, we measure a zeta potential of $\zeta = (-29.1 \pm 0.4)$ mV (Figure 1e). As the probes are negatively charged, the zeta potential becomes more negative if more probes are immobilized on the surface. The measured diameters are consistent with a common average value $d = 71 \pm 3\,\mathrm{nm}$ for all samples, and the value agrees with DLS measurement performed on bare liposomes (Figure S3). This indicates that the probes do not cause significant clustering of the liposomes. In case of clustering, the spatial distribution in the trap would narrow significantly as an increase in particle size causes a smaller diffusion coefficient.

The net surface charge on the liposomes can be estimated from their zeta potentials (Ref. [32], eq 2.5.5). The estimated surface charges are shown in Figure 1f. A linear fit shows that the surface charge increase by $(0.73 \pm 0.10)e$ per added probe. For the DNA probe lengths used here, the detection limit is down to ~ 40 functionalized probes per liposome, corresponding to $\sim 25\,e$ or a $\sim 1.5\%$ change in liposome net surface charge. The method can thus be used to evaluate the functionalization of liposomes with DNA probes when the functionalization is performed outside of the device.

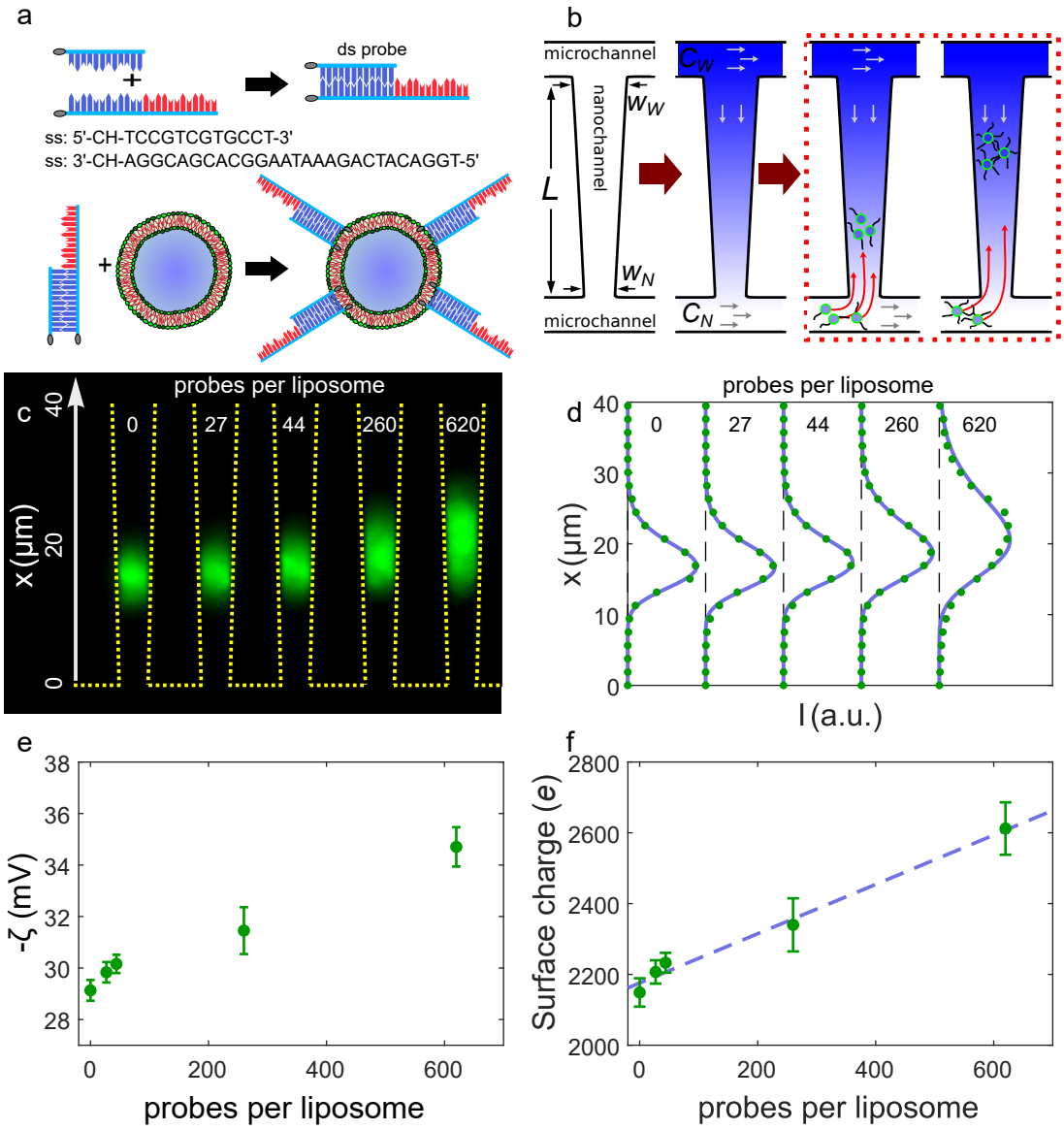

Figure 1: (a) Schematic of the DNA probe constructs from two ssDNA molecules and their immobilization on the surface of liposomes via cholesterol. (b) Schematic of the sensor for nanoparticle trapping. The widths of the two ends of the nanochannels are $w_N = 5\,\mu m$ and $w_W = 20\,\mu m$, the length is $L = 440\,\mu m$, and the height is $h = 295\,nm$. Different salt concentrations in the two microchannels establish a salt gradient in the nanochannel. Liposomes introduced in the microchannel migrate to the nanochannel and are trapped due to a balance between the diffusioosmotic flow and the diffusiophoretic velocity of the liposomes. The trapping position depends on the particle size and zeta potential, and, consequently, the number of probes immobilized on the surface. (c) Composite fluorescence image of five individual measurements of liposome samples with different numbers of probes averaged over 10 s. Liposomes with a higher number of probes on the surface are trapped further into the nanochannel. (d) Average fluorescence intensity along the nanochannels for the data shown in Panel d (green dots). Full, blue lines are independent fits to eq 1. Fit parameters are the zeta potential ζ and the diameter d. (e) Fitted zeta potentials from the fits in Panel c (green dots). (f) Linear fit (dashed blue line) to the surface charge (green dots) versus the number of probes per liposome.

We now monitor in real-time the binding of unlabelled ssDNA targets to the probes immobilized on the liposomes. The DNA targets are 15mer oligos complementary to the single-stranded overhang of the probes on the liposome surfaces (Figure 2a). Hybridization of the target has a dissociation constant $K_d \sim 2.5\,\mathrm{pM}$ and can thus be considered irreversible at the used target concentration.

First, an ensemble of liposomes with a known number of probes immobilized on the surface is trapped as described above. When the spatial distribution of liposomes in the nanochannel is stable, we exchange the solution in one of the microchannels from a solution with liposomes to a 10 nM solution of DNA targets. This gives a DNA target concentration of approximately 9 nM at the liposomes' trapping position (see equation 1 in Supporting Information). We maintain at all time the same salt concentration in the microchannels, so the salt gradient is unaffected by the exchange of solution and liposomes remain trapped (see Figure 2b). The DNA targets diffuse into the nanochannels and hybridize to the probes on the liposomes. A time-lapse shows the spatial distribution of an ensemble of trapped liposomes with an average of 260 probes per liposome when DNA targets are introduced at time $t = 1$ min (Figure 2c). We observe the reaction between the targets and the probes as it occurs, as the net charge of the liposomes increases upon hybridization and, consequently, shifts the trapping position further into the nanochannel.

The red dots in Figure 2d mark the intensities averaged across the nanochannel at different time points. The full, blue lines are fits to eq 1 from which we extract the size and the zeta potential of the liposomes. Fits are performed in two steps: First, we fit with both the zeta potential ζ and the diameter d as free parameters. As the diameters for different time points are consistent with a common average value $d_{\mathrm{avg}} = (73 \pm 3)\,\mathrm{nm}$ (Figure S4), we fix the diameter at this value and make a new fit for the different time points with the zeta potentials as the only free parameter.

Figure 2e shows the time dependence of the zeta potential during hybridization for ensembles of liposomes with different numbers of DNA probes. The zeta potential of the bare

liposomes do not change, indicating no significant unspecific binding between the target and the lipid bilayer of the liposomes. For liposomes with DNA probes, the zeta potential increases after introduction of the complementary target at $\sim 1\,\mathrm{min}$ for the three samples with the highest number of probes (44, 260 and 620). After $\sim 3\,\mathrm{min}$, the zeta potential saturates, indicating that all probes on the liposomes have hybridized with a target. For the liposomes with fewest probes (27 per liposome), no significant change in zeta potential is observed. So the detection limit for the assay is between 27 and 44 DNA probes, which corresponds to $\sim 30e$ for the sample with 44 probes. Again, this is a 1.5% change in the liposome net surface charge.

We plot the estimated surface charge per liposome as a function of the number of probes per liposome at time $t = 0$ and $t = 4\,\mathrm{min}$, that is before and after the reaction, respectively (Figure 2f). As expected, the surface charge is proportional to the number of probes. Linear fits give that the surface charge of a liposome increases by $(0.66 \pm 0.06)\,e$ per added probe and that the surface charge increase additionally by $q_{\mathrm{target}}(0.48 \pm 0.10)\,e$ per target hybridized on the probes. This corresponds to a charge of $(0.040 \pm 0.004)e$ per base pair for each hybridized probe-target pair on the liposome. The value is consistent with thermophoretic measurements on short DNA molecules[19] and gel electrophoresis[33].

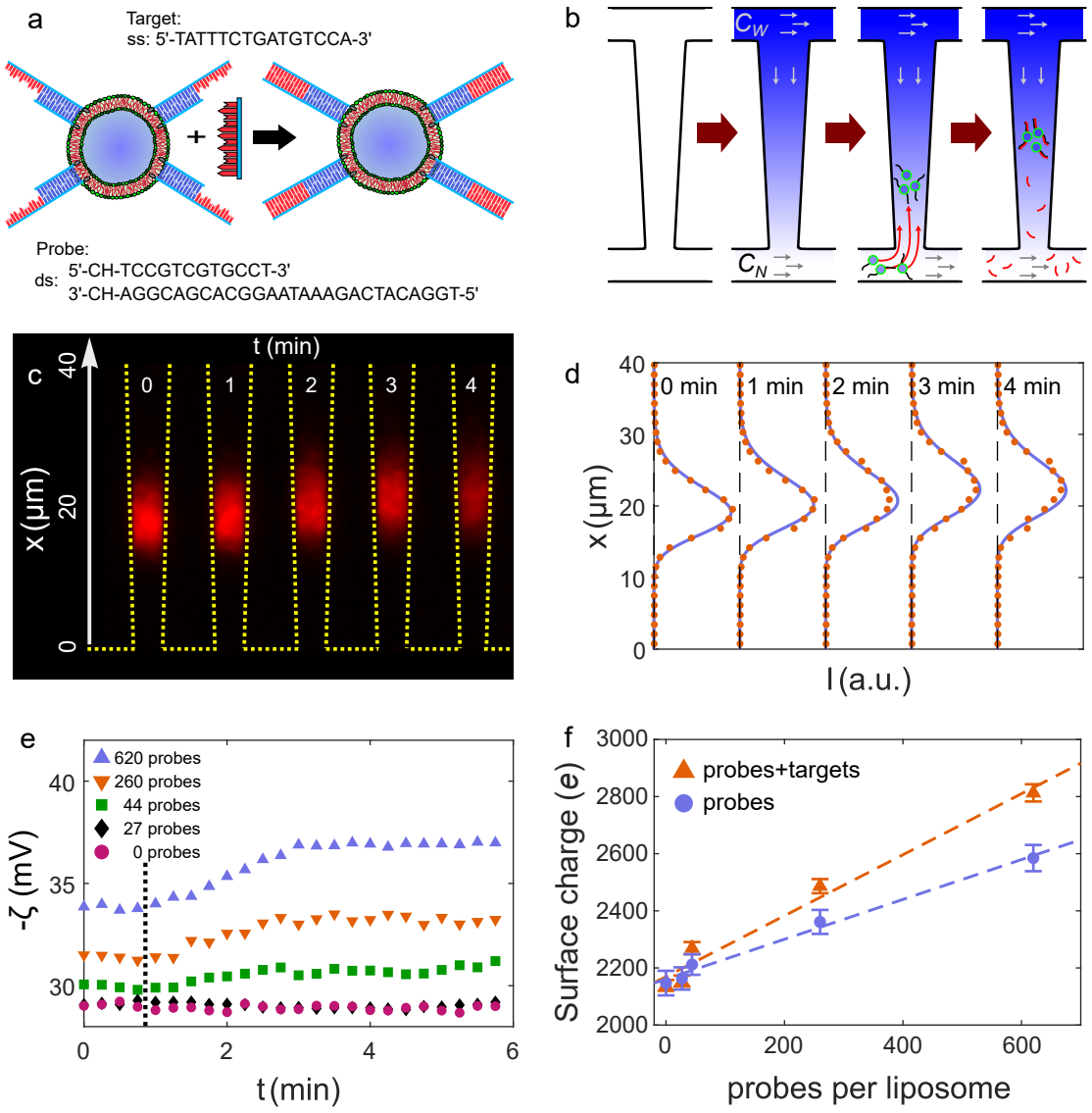

Figure 2: (a) Schematic of the hybridization of ssDNA targets to DNA probes on the surface of liposomes. (b) Schematic of the method for detecting hybridization of ssDNA targets on liposomes decorated with DNA probes. First, a salinity gradient is established and the liposomes with probes are trapped. Then targets are introduced, and as they react with probes, the liposomes change position. (c) Composite time-lapse fluorescence images averaged over 15 s of the liposomes with 260 probes per liposome during the hybridization of the target. Targets are introduced just before $t \sim 1$ min. The liposomes move further into the nanochannel as the probes and the targets form pairs. (d) Intensity along the nanochannel (red dots) and fits (blue line) at different time points. (e) Fitted values for the zeta potential as a function of time for the five samples. The black, dashed line indicates when the target arrive at the nanochannels. (f) Fitted net surface charges on the liposomes before (blue) and after (red) the reaction occurs.

In our experiments, the surfaces of the liposomes are almost identical, so we expect a

fixed average number of probes per area, and consequently, that the number of probes per liposome follows Poisson statistics. So for a high average number of probes per liposome, the hybridization kinetics of the individual liposomes will be similar to the kinetics of the ensemble. In contrast, if the ensemble of liposomes is heterogeneous with respect to the number of probes, only the hybridization kinetics for the individual liposomes can resolve this heterogeneity. So we populate nanochannels with single liposomes by establishing the salinity gradient in the nanochannels and then introduce a dilute sample of liposomes in the microchannel. This allows for trapping of individual liposomes in the nanochannels. Similar to the measurements on ensembles (Figure 2), the targets are introduced in the microchannel, diffuse into the traps, and bind to the liposomes.

Single-particle tracking was done for a total of 88 liposomes from three different ensembles (28 were control liposomes with no probes, 33 liposomes had 260 probes per liposome, and 27 liposomes had 260 probes per liposome and were hybridized with targets in the nanofluidic sensor). Figure 3a shows typical histograms of the x-coordinate for 40 s measurement series for the three different types of liposomes. Assuming that the distribution of x-coordinates is similar to the distribution of positions for an ensemble of liposomes, we fit eq 1 to the histograms (full blue lines). The fitted values for the diameters are for all liposomes consistent with a common average value (Figure S5), so the only difference between the ensembles is their zeta potentials. Figure 3b shows the fitted values for the zeta potential for control liposomes without probes (black), with probes (green), and with probes after hybridization with targets (red). The first data point in each series corresponds to the liposome data shown in Figure 3a. The averages of the zeta potentials for the individual liposomes (dashed lines) are consistent with the values obtained for the ensembles in Figure 2 (solid blue lines). This shows that we can reliably extract the size and zeta potential from measurement on individual liposomes before and after hybridization.

The entire hybridization process is also monitored for a single liposome with 260 probes. The shift in trapping position induced by the change of zeta potential is clearly visible from the liposome positions shown in Figure 3c before (green) and after (red) the hybridization with targets. The x-coordinates of the liposomes during the entire experiment is shown in Figure 3d, i.e., from trapping, during hybridization, and, finally, saturation of the probes. The targets are introduced via the microchannel and reach the nanochannels at time $t \sim 20\,\mathrm{s}$ where they diffuse into the nanochannels. Consequently, the trapping position of the liposome shifts as the target and probes hybridize. The average position before (green) and after (red) the reaction are marked with dashed lines. Figure 3e shows the histograms of the x-coordinate of the liposome from Figure 3d before and after the reaction. They allow us to quantify the shift in trapping positions due to hybridization. The full blue lines are fits to eq 1. The fitted zeta potentials before and after the reaction are $\zeta_{\mathrm{before}} = (-31.3 \pm 0.7)\,\mathrm{mV}$ and $\zeta_{\mathrm{after}} = (-33.2 \pm 0.5)\,\mathrm{mV}$, respectively, and the diameter is estimated to $d = (72 \pm 5)\,\mathrm{nm}$. The number of targets bound to the probes on the surface is, for this particular liposome, $n_{\mathrm{target}} = \frac{q_{\mathrm{after}} - q_{\mathrm{before}}}{q_{\mathrm{target}}} = 300 \pm 90$. Here $q_{\mathrm{before}} = (2340 \pm 40)\,e$ and $q_{\mathrm{after}} = (2490 \pm 30)\,e$ are the net surface charges calculated from ζ_{before} and ζ_{after}, respectively, using Ref. [32], eq 2.5.5. The value $q_{\mathrm{target}} = (0.48 \pm 0.10)e$ is the net charge added per target, obtained from Figure 2f.

CONCLUSION

We have used a diffusiophoretic trap as a sensor to monitor the surface charge of individual and ensembles of liposomes during ligand binding. The sensitivity to changes in surface charge is down to 1.5 % of the total surface charge. We used cholesterol anchors to functionalize the liposomes with DNA probes and hybridization of short DNA targets to demonstrate the capability of real-time monitoring of biomolecular recognition at physiological conditions. DNA probes and targets is an ideal system due to the well-characterized affinity and tunable

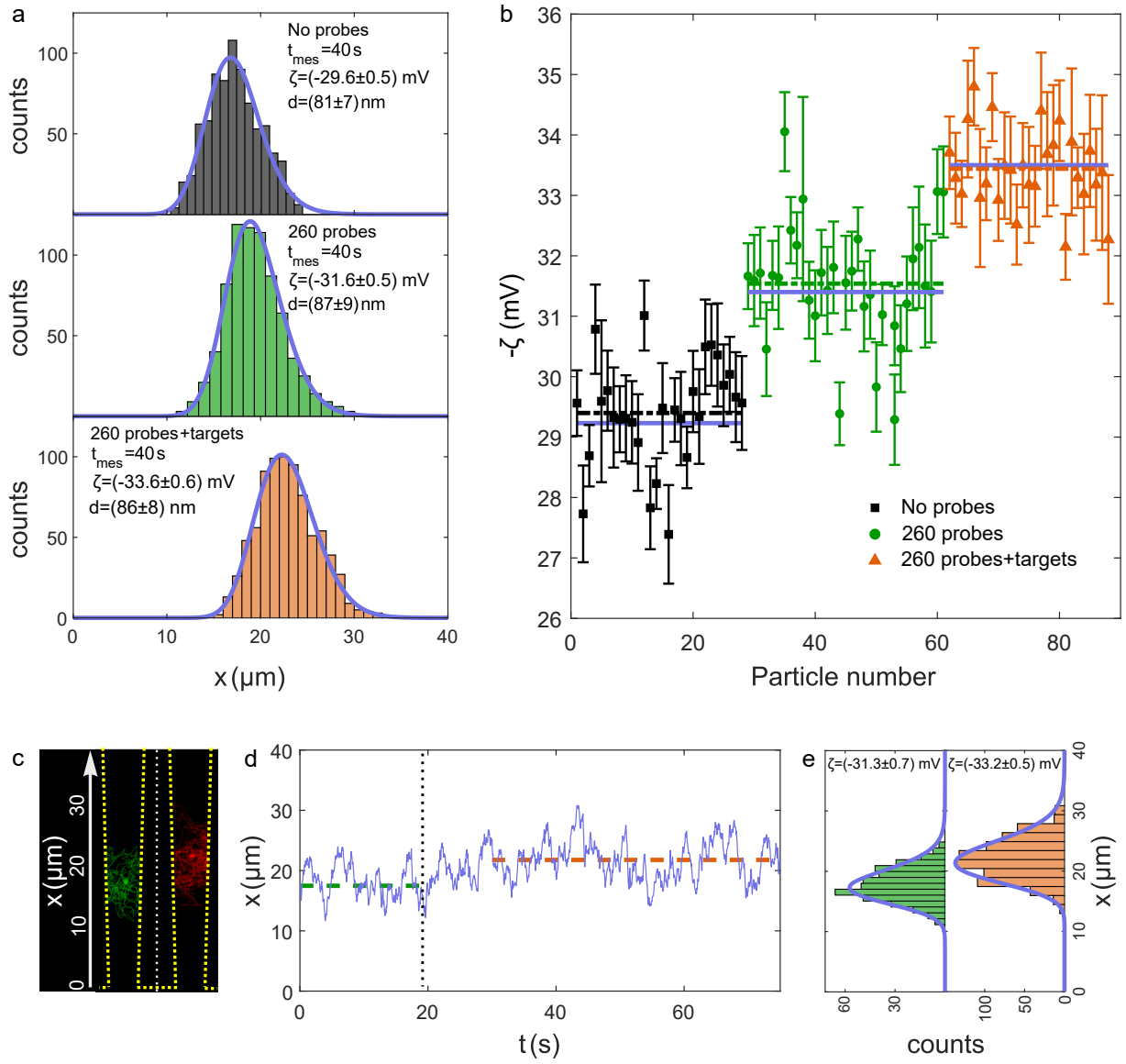

Figure 3: (a) Histograms of the x-coordinates and fits to eq 1 for a liposome without probes (top), a liposome with 260 probes (middle), and a liposome with both 260 probes and targets after hybridization (bottom). (b) Zeta potential for individual liposomes from samples without probes, with 260 probes, and with both 260 probes and targets after hybridization. Their respective mean values are marked with dashed lines. Full blue lines are ensemble averages from Figure 2. The first point in each series corresponds to the liposomes shown in Panel a. (c) Positions of a liposome with 260 probes in the trap before (green) and after (red) hybridization of the targets. (d) x-coordinate of a single liposome before, during, and after the hybridization of the targets (blue line). The average trapping positions before and after the reaction are marked with dashed green and red lines, respectively. The arrival of targets at the nanochannel entry is marked with a black, dashed line. (e) Histogram of the x-coordinates for the particle in Panel a and fits to eq 1 before (green) and after (red) the reaction occurs. Fitted values for the zeta potentials are stated in the figure.

kinetics.

With the sensor, we could detect surface charge changes down to $\sim 25\,e$, i.e. down to ~ 40 probes per liposome. This is comparable to other label-free charge-based methods such as TRPS and SHG. For TRPS, detection of down to ~ 40 DNA strings per liposome has been reported for DNA strings with 35 bases [34]. For both our sensor and TRPS, the sensitivity to the number of probes depends on the probe length, as longer probes carry more charge. SHG sensitivities of ~ 10 transacting activator of transduction (TAT) peptides binding to 200 nm liposomes have been measured [20]. TAT peptides each carry eight charges, so the reported sensitivity is $\sim 80\,e$.

The sensor presented here is applicable as a quality control for liposomes decorated with nucleic acids for drug delivery, as the functionalization efficiency can be inferred from the change in surface charge upon binding with the complementary target. Unintended effects of the binding, such as aggregation of liposomes, can also be detected since the sizes of the liposomes are tracked during the reaction. The label-free sensing based on monitoring the zeta potential can be applied to any binding reaction that changes the net surface change.

Applications within diagnostics based on characterizing the binding properties of biocolloids can also be envisioned. For example, exosomes from liquid biopsies play an important role in diagnostic methods for several diseases, including cancer [35]. The exosomes carry proteins, mRNA, and antigens on the surfaces which serve as biomarkers. The detection and quantification of these surface markers could be accomplished with the sensor presented here.

The lipid-based coating currently used for passivation of the nanofluidic sensor prevents sticking to the channel surface for the liposomes used in this work and for exosomes [26]. Characterizing the properties of non-lipid-based nanoparticles, such as gold or polymer nanoparticles, will require the development of new coatings. Such coatings will change the channel's surface charge and, consequently, the diffusioosmotic velocity in the nanochannel. The sensitivity of the sensor with respect to changes in the zeta potential during a reaction could then

also be increased by tuning the diffusioosmotic velocity or the dimensions of the channel, as a larger effective width of the trap increases the sensitivity.

EXPERIMENTAL SECTION

Liposome synthesis

Liposomes were prepared by lipid film hydration. First, POPC and POPG lipids were dissolved in a 9:1 tertiary butanol to H_2O solution and mixed with the membrane fluorophore DiO to obtain a POPC:POPG 3:1 mixture. The mixture was then freeze dried for 24 hours. The resulting lipid film was then rehydrated with PBS and kept at 50 °C while being vortexed every 15 minutes for an hour. Finally, the sample was extruded through polycarbonate membranes with 30 nm holes to create liposomes with a mean diameter of 76 nm (measured by DLS).

DNA hybridization and immobilization

The double-stranded DNA probes were hybridized by mixing two single-stranded DNA molecules with 12 and 27 base pairs and cholesterol anchors at the 3' and 5' ends, respectively (5'-CH-TCCGTCGTGCCT-3' and 3'-CH-AGGCAGCACGGAATAAAGACTACAGGT-5' purchased from Biomers). The mixture was then incubated at 30 °C for an hour. The two single-strands were complementary such that the two cholesterol anchors are at the same end of the double-stranded DNA probe.

The probes were immobilized on the liposome surfaces by simple mixing and were then kept at 4 °C for 24 h.

Nanofluidic sensor fabrication

The nanofluidic sensor was injection molded in the cyclic olefin polymer (COC) TOPAS 5013 using a nickel master produced in a two-step UV-lithography and reactive ion etching process [36]. The microchannels were made with a height of 5 µm and connected by 16 parallel nanochannels with a height of 295 nm. The injection molded part was sealed with a 150 µm thick COC foil by UV-assisted thermal bonding.

Nanofluidic experiments

The device surfaces were passivated by coating with a mixture of POPC:POPG 3:1 dissolved in 70% ethanol for 30 minutes. The salinity gradient used in the trapping and hybridization experiments was maintained by a continuous flow of PBS in the microchannels with concentrations of $C_N = 10^{-3}\times$PBS and $C_W = 10\times$PBS. The flows were driven by a 5 mbar pressure difference between the ends of the microchannels and were controlled by a Fluigent MFCS-EX.

Liposomes are introduced in a solution of $C_N = 10^{-3}\times$PBS and get trapped in the nanochannel. After $\sim$ 2 minutes, the supply of liposomes is stopped by changing to a pure $C_N = 10^{-3}\times$PBS solution. The trapped liposomes are imaged with a capture rate of 20 images per second with an exposure time of 50 ms using a Nikon eclipse Ti2 microscope with a Photometrics Evolve 512 electron-multiplying charge-coupled device camera. For the hybridization experiments, a solution with $C_N = 10^{-3}\times$PBS and 10 nM single-stranded DNA targets is introduced in the microchannel with the low salt concentration.

Associated content

Supporting information

Details on salt gradient, diffusiophoresis and diffusioosmosis in the nanofluidic sensor. Characterization of number of probes on liposome ensembles. Diameters obtained from trapping experiments.

Supporting Movie

Liposomes with 620 probes getting trapped in a nanochannel by a salinity gradient.

Author Contribution

R.M. and J.N.P. developed the project and led the experimental research. M.K.R. and J.N.P. developed the theory predicting the behaviour of functionalized liposomes in the trap. M.K.R performed the experiments. All authors analyzed data and co-wrote the manuscript.

Notes

The authors declare no competing interest.

References

(1) Sercombe, L.; Veerati, T.; Moheimani, F.; Wu, S. A. K., Sherry Y; Hua, S. Advances and challenges of liposome assisted drug delivery. *Frontiers in pharmacology* **2015**, *6*, 286.

(2) Wang, Z.; Deng, X.; Ding, J.; Zhou, W.; Zheng, X.; Tang, G. Mechanisms of drug

release in pH-sensitive micelles for tumour targeted drug delivery system: A review. *International Journal of Pharmaceutics* **2018**, *535*, 253–260.

(3) Rideau, E.; Dimova, R.; Schwille, P.; Wurm, F. R.; Landfester, K. Liposomes and polymersomes: a comparative review towards cell mimicking. *Chemical Society Reviews* **2018**, *47*, 8572–8610.

(4) Jølck, R. I.; Feldborg, L. N.; Andersen, S.; Moghimi, S. M.; Andresen, T. L. *Biofunctionalization of Polymers and their Applications*; Springer, 2010; pp 251–280.

(5) Lopez, A.; Liu, J. DNA oligonucleotide-functionalized liposomes: bioconjugate chemistry, biointerfaces, and applications. *Langmuir* **2018**, *34*, 15000–15013.

(6) Re, F.; Cambianica, I.; Zona, C.; Sesana, S.; Gregori, M.; Rigolio, R.; La Ferla, B.; Nicotra, F.; Forloni, G.; Cagnotto, A. et al. Functionalization of liposomes with ApoE-derived peptides at different density affects cellular uptake and drug transport across a blood-brain barrier model. *Nanomedicine: Nanotechnology, Biology and Medicine* **2011**, *7*, 551–559.

(7) Chen, C.; Duan, Z.; Yuan, Y.; Li, R.; Pang, L.; Liang, J.; Xu, X.; Wang, J. Peptide-22 and cyclic RGD functionalized liposomes for glioma targeting drug delivery overcoming BBB and BBTB. *ACS applied materials & interfaces* **2017**, *9*, 5864–5873.

(8) Ohradanova-Repic, A.; Nogueira, E.; Hartl, I.; Gomes, A. C.; Preto, A.; Steinhuber, E.; Mühlgrabner, V.; Repic, M.; Kuttke, M.; Zwirzitz, A. et al. Fab antibody fragment-functionalized liposomes for specific targeting of antigen-positive cells. *Nanomedicine: Nanotechnology, Biology and Medicine* **2018**, *14*, 123 – 130.

(9) Eloy, J. O.; Petrilli, R.; Trevizan, L. N. F.; Chorilli, M. Immunoliposomes: a review on functionalization strategies and targets for drug delivery. *Colloids and Surfaces B: Biointerfaces* **2017**, *159*, 454–467.

(10) Löffler, P. M.; Ries, O.; Rabe, A.; Okholm, A. H.; Thomsen, R. P.; Kjems, J.; Vogel, S. A DNA-Programmed Liposome Fusion Cascade. *Angewandte Chemie International Edition* **2017**, *56*, 13228–13231.

(11) Stengel, G.; Zahn, R.; Höök, F. DNA-induced programmable fusion of phospholipid vesicles. *Journal of the American Chemical Society* **2007**, *129*, 9584–9585.

(12) Tiriveedhi, V.; Butko, P. A fluorescence spectroscopy study on the interactions of the TAT-PTD peptide with model lipid membranes. *Biochemistry* **2007**, *46*, 3888–3895.

(13) Olaru, A.; Bala, C.; Jaffrezic-Renault, N.; Aboul-Enein, H. Y. Surface plasmon resonance (SPR) biosensors in pharmaceutical analysis. *Critical reviews in analytical chemistry* **2015**, *45*, 97–105.

(14) Qiu, F.; Mhanna, R.; Zhang, L.; Ding, Y.; Fujita, S.; Nelson, B. J. Artificial bacterial flagella functionalized with temperature-sensitive liposomes for controlled release. *Sensors and Actuators B: Chemical* **2014**, *196*, 676–681.

(15) Shimanouchi, T.; Ishii, H.; Yoshimoto, N.; Umakoshi, H.; Kuboi, R. Calcein permeation across phosphatidylcholine bilayer membrane: effects of membrane fluidity, liposome size, and immobilization. *Colloids and Surfaces B: Biointerfaces* **2009**, *73*, 156–160.

(16) Hatzakis, N. S.; Bhatia, V. K.; Larsen, J.; Madsen, K. L.; Bolinger, P.-Y.; Kunding, A. H.; Castillo, J.; Gether, U.; Hedegård, P.; Stamou, D. How curved membranes recruit amphipathic helices and protein anchoring motifs. *Nature chemical biology* **2009**, *5*, 835–841.

(17) Putta, P.; Rankenberg, J.; Korver, R. A.; van Wijk, R.; Munnik, T.; Testerink, C.; Kooijman, E. E. Phosphatidic acid binding proteins display differential binding as a function of membrane curvature stress and chemical properties. *Biochimica et Biophysica Acta (BBA)-Biomembranes* **2016**, *1858*, 2709–2716.

(18) Zhang, H.; Freitas, D.; Kim, H. S.; Fabijanic, K.; Li, Z.; Chen, H.; Mark, M. T.; Molina, H.; Martin, A. B.; Bojmar, L. et al. Identification of distinct nanoparticles and subsets of extracellular vesicles by asymmetric flow field-flow fractionation. *Nature Cell Biology* **2018**, *20*, 332–343.

(19) Duhr, S.; Braun, D. Why molecules move along a temperature gradient. *Proceedings of the National Academy of Sciences* **2006**, *103*, 19678–19682.

(20) Rao, Y.; Kwok, S. J.; Lombardi, J.; Turro, N. J.; Eisenthal, K. B. Label-free probe of HIV-1 TAT peptide binding to mimetic membranes. *Proceedings of the National Academy of Sciences* **2014**, *111*, 12684–12688.

(21) Goyon, A.; Excoffier, M.; Janin-Bussat, M.-C.; Bobaly, B.; Fekete, S.; Guillarme, D.; Beck, A. Determination of isoelectric points and relative charge variants of 23 therapeutic monoclonal antibodies. *Journal of Chromatography B* **2017**, *1065*, 119–128.

(22) Chi, Y.; Yin, X.; Sun, K.; Feng, S.; Liu, J.; Chen, D.; Guo, C.; Wu, Z. Redox-sensitive and hyaluronic acid functionalized liposomes for cytoplasmic drug delivery to osteosarcoma in animal models. *Journal of Controlled Release* **2017**, *261*, 113–125.

(23) Blundell, E. L.; Mayne, L. J.; Billinge, E. R.; Platt, M. Emergence of tunable resistive pulse sensing as a biosensor. *Analytical Methods* **2015**, *7*, 7055–7066.

(24) Mojarad, N.; Krishnan, M. Measuring the size and charge of single nanoscale objects in solution using an electrostatic fluidic trap. *Nature Nanotechnology* **2012**, *7*, 448.

(25) Ruggeri, F.; Zosel, F.; Mutter, N.; Różycka, M.; Wojtas, M.; Ożyhar, A.; Schuler, B.; Krishnan, M. Single-molecule electrometry. *Nature Nanotechnology* **2017**, *12*, 488.

(26) Rasmussen, M. K.; Pedersen, J. N.; Marie, R. Size and surface charge characterization of nanoparticles with a salt gradient. *Nature communications* **2020**, *11*, 1–8.

(27) Anderson, J. L. Colloid transport by interfacial forces. *Annual Review of Fluid Mechanics* **1989**, *21*, 61–99.

(28) Pfeiffer, I.; Höök, F. Bivalent cholesterol-based coupling of oligonucletides to lipid membrane assemblies. *Journal of the American Chemical Society* **2004**, *126*, 10224–10225.

(29) Lee, C.; Cottin-Bizonne, C.; Biance, A.-L.; Joseph, P.; Bocquet, L.; Ybert, C. Osmotic flow through fully permeable nanochannels. *Physical Review Letters* **2014**, *112*, 244501.

(30) Prieve, D. C.; Anderson, J. L.; Ebel, J. P.; Lowell, M. E. Motion of a particle generated by chemical gradients. Part 2. Electrolytes. *Journal of Fluid Mechanics* **1984**, *148*, 247–269.

(31) Happel, H., J. & Brenner *Low Reynolds Number Hydrodynamics*; Prentice Hall, 1965.

(32) Hunter, R. *Zeta potential in colloid science. Principles and Applications*; Academic Press, 1981.

(33) Smith, S. B.; Bendich, A. J. Electrophoretic charge density and persistence length of DNA as measured by fluorescence microscopy. *Biopolymers: Original Research on Biomolecules* **1990**, *29*, 1167–1173.

(34) Vogel, R.; Pal, A. K.; Jambhrunkar, S.; Patel, P.; Thakur, S. S.; Reátegui, E.; Parekh, H. S.; Saá, P.; Stassinopoulos, A.; Broom, M. F. High-Resolution Single Particle Zeta Potential Characterisation of Biological Nanoparticles using Tunable Resistive Pulse Sensing. *Scientific Reports* **2017**, *7*, 17479.

(35) Skog, J.; Würdinger, T.; Van Rijn, S.; Meijer, D. H.; Gainche, L.; Curry, W. T.; Carter, B. S.; Krichevsky, A. M.; Breakefield, X. O. Glioblastoma microvesicles transport RNA and proteins that promote tumour growth and provide diagnostic biomarkers. *Nature cell biology* **2008**, *10*, 1470–1476.

(36) Utko, P.; Persson, F.; Kristensen, A.; Larsen, N. B. Injection molded nanofluidic chips: fabrication method and functional tests using single-molecule DNA experiments. *Lab on a Chip* **2011**, *11*, 303–308.